Valley-Free Silicon Fins Caused by Shear Strain

Christoph Adelsberger,* Stefano Bosco,† Jelena Klinovaja, and Daniel Loss
Department of Physics, University of Basel, Klingelbergstrasse 82, CH-4056 Basel, Switzerland

(Received 25 August 2023; revised 4 April 2024; accepted 5 June 2024; published 17 July 2024)

Electron spins confined in silicon quantum dots are promising candidates for large-scale quantum computers. However, the degeneracy of the conduction band of bulk silicon introduces additional levels dangerously close to the window of computational energies, where the quantum information can leak. The energy of the valley states—typically 0.1 meV—depends on hardly controllable atomistic disorder and still constitutes a fundamental limit to the scalability of these architectures. In this work, we introduce designs of complementary metal-oxide-semiconductor (CMOS)-compatible silicon fin field-effect transistors that enhance the energy gap to noncomputational states by more than one order of magnitude. Our devices comprise realistic silicon-germanium nanostructures with a large shear strain, where troublesome valley degrees of freedom are completely removed. The energy of noncomputational states is therefore not affected by unavoidable atomistic disorder and can further be tuned *in situ* by applied electric fields. Our design ideas are directly applicable to a variety of setups and will offer a blueprint toward silicon-based large-scale quantum processors.

DOI: 10.1103/PhysRevLett.133.037001

Introduction.—Spins in silicon and germanium quantum dots (QDs) are workhorses of modern semiconductor-based quantum technology [1–12]. The most advanced platforms to date utilize planar heterostructures comprising Si and SiGe alloys, where quantum information is carried by single electrons confined in the Si layer [9–13]. In these systems, long spin coherence is enabled by the weak spin-orbit interaction of the conduction band and by isotopically purifying Si [14]. Electron spin resonance was harnessed to selectively control individual qubits [15–17] whereas tunable exchange interactions mediate fast, high-fidelity two-qubit gates [8,18–23]. The versatility of these architectures permitted remote coupling of distant qubits via microwave cavities [24–26] and spin shuttling [27–30], as well as entanglement of three spin states [31]. Readout and two-qubit gate fidelities exceeding the error correction threshold [13,32–34] and the recent demonstration of six-qubit quantum processors [9] constitute promising steps toward large-scale quantum processors.

Further progress in electron spin qubits in silicon is currently hindered by the valley degeneracy of the silicon conduction band. In planar Si/SiGe heterostructures tensile in-plane strain partially lifts the six-fold degeneracy of bulk silicon, pushing four valleys to higher energy; the ground state remains twofold degenerate [35–37]. The residual valleys introduce troublesome additional levels in the vicinity of the computational energies where the quantum information is processed. These states open the system to decoherence and relaxation channels and constitute a critical source of leakage [38–45]. The valley degeneracy can be lifted by strong electric fields, but the induced energy gap is relatively small 10–100 μeV and dangerously close to the typical qubit energies ∼10 μeV. Because it strongly depends on atomistic details of the Si/SiGe interface, controlling this gap reliably and reproducibly is challenging [46–52]. Moreover, in hot qubits, valley states can be thermally excited, hindering the scalability of quantum processors [53]. Larger valley splittings are reached by periodically altering the concentration of Ge in the well [54,55]. In metal-oxide-semiconductor (MOS) structures, splittings ∼0.5 meV are reached by tightly confined electrons at the interfaces between Si and SiO_2, but these values largely depend on interface disorder [53,56–58].

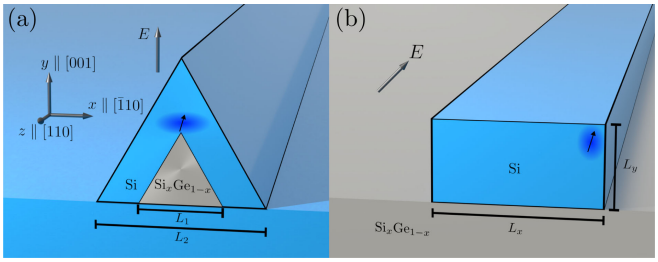

FIG. 1. Design of valley-free fins in Si/Si$_x$Ge$_{1-x}$ heterostructures. (a) Equilateral triangular fin with inner and outer side lengths L_1 and L_2, respectively. The wave function is localized in the Si shell by uniaxial strain and the electric field $\boldsymbol{E}$. The fin is assumed to be grown on a Si substrate, but the results are similar for a Ge substrate. (b) Rectangular Si slab with side lengths L_x and L_y on Si$_x$Ge$_{1-x}$ substrate. The electrons are confined at the corners by $\boldsymbol{E}$ in the x-y plane. The blue dots show the position of the QD hosting the spin qubit. We assume infinitely long systems in the z direction. The coordinate system in (a) shows the crystallographic growth directions for both geometries.

 © 2024 American Physical Society

In this work, we propose alternative Si/SiGe nanostructures that completely lift the valley degeneracy and thus provide ideal platforms for future spin-based quantum processors. In our designs the electrons are confined in quasi-one-dimensional (1D) Si fins compatible with CMOS technology [59], see Fig. 1, where, in contrast to planar heterostructures, the SiGe induces a large *shear* strain. The growth of similar fin structures as in Fig. 1(a) has been demonstrated in Ref. [60]. By detailed simulations based on continuum elasticity theory and microscopic $\boldsymbol{k}\cdot\boldsymbol{p}$ theory, we show that our engineered strain profile enables a nondegenerate ground state split from the excited states by energies ∼1–10 meV, 2 to 3 orders of magnitude larger than in current devices. Importantly, this energy gap remains large for realistic values of applied electric fields and is independent of atomistic disorder at the interfaces, rendering our design robust in a wide variety of different fins.

Theoretical model.—The conduction band of bulk Si has six degenerate minima in the first Brillouin zone (BZ), which are located at distance $\pm k_0/2\pi = \pm 0.15/a_{\mathrm{Si}}$ from the X points (Si lattice constant $a_{\mathrm{Si}} = 5.43$ Å [61]). Its low-energy electronic states are described by the microscopic two-band $\boldsymbol{k}\cdot\boldsymbol{p}$ Hamiltonian [62,63]:

$$H = \frac{\hbar^2}{2m_t}\left(k_{t_1}^2 + k_{t_2}^2\right) + \frac{\hbar^2}{2m_l}k_l^2 + \Xi_u\varepsilon_{ll} + e\boldsymbol{E}\cdot\boldsymbol{r} + V(\boldsymbol{r}) + \frac{\hbar^2}{m_l}k_0 k_l \tau_x - \left(\frac{\hbar^2}{M}k_{t_1}k_{t_2} - 2\Xi_{u'}\varepsilon_{t_1t_2}\right)\tau_z, \quad (1)$$

where l is the longitudinal direction, and t_1 and t_2 are the transversal directions, which are aligned with the main crystallographic axes [100], [010], and [001]. The canonical momentum operators are $\hbar k_j = -i\hbar\partial_j$ $(j = l, t_1, t_2)$.

This Hamiltonian is based on a small-momentum expansion of the band structure around the X points and the Pauli matrices τ_i $(i = x, y, z)$ refer to the two bands crossing there. Because there are three inequivalent X points, the six valleys are described by three independent copies of Eq. (1). The spin degree of freedom is neglected in H. The transversal and longitudinal masses are $m_t = 0.19m_e$ and $m_l = 0.91m_e$, respectively, with the free electron mass m_e; $M \approx (m_t^{-1} - m_e^{-1})^{-1}$ is the band-coupling mass [62,64].

The lattice constant of Ge $a_{\mathrm{Ge}} = 5.66$ Å [61] is larger than a_{Si}. Thus, the Si is strained in Si/SiGe heterostructures. The uniaxial strain ε_{ll} and the shear strain $\varepsilon_{t_1t_2}$ modify the electron energy depending on the deformation potentials $\Xi_u = 9$ eV [65–71] and $\Xi_{u'} = 7$ eV [62,72,73], respectively. In the nanostructures sketched in Fig. 1, we simulate the strain tensor elements $\underline{\boldsymbol{\varepsilon}}$ by finite-element methods (FEM) based on continuum elasticity theory [74–77]. A short review of linear elasticity theory and details on strain simulations is provided in the Supplemental Material (SM) [78]. We assume that the lattice constant of an alloy of $\mathrm{Si}_x\mathrm{Ge}_{1-x}$ changes linearly from a_{Si} to a_{Ge}, and thus we use the relation

$$\underline{\boldsymbol{\varepsilon}}_{\mathrm{Si/Si}_x\mathrm{Ge}_{1-x}} = (1-x)\underline{\boldsymbol{\varepsilon}}_{\mathrm{Si/Ge}}, \quad (2)$$

interpolating linearly from the minimal strain at $1-x=0$ to the maximal strain at $1-x=1$, which is a good approximation for the actual relation [70,82,83].

Equation (1) includes the homogeneous electric field $\boldsymbol{E}$ resulting in the electrostatic potential $-e\boldsymbol{E}\cdot\boldsymbol{r}$, with the electron charge $e>0$, $\boldsymbol{r} = (x, y, z)$, and the confinement potential $V(\boldsymbol{r})$. We model the sharp interface between Si and a $\mathrm{Si}_x\mathrm{Ge}_{1-x}$ alloy by using the steplike potential function

$$V(\boldsymbol{r}) = \begin{cases} 0 & \text{for } \boldsymbol{r}\in R_{\mathrm{Si}}, \\ (1-x)500\ \mathrm{meV} & \text{for } \boldsymbol{r}\in R_{\mathrm{Si}_x\mathrm{Ge}_{1-x}}, \end{cases} \quad (3)$$

where R_{Si} $(R_{\mathrm{Si}_x\mathrm{Ge}_{1-x}})$ indicates the region in the cross section occupied by Si ($\mathrm{Si}_x\mathrm{Ge}_{1-x}$). In analogy to Eq. (2), we also assume that $V(\boldsymbol{r})$ decreases linearly from the maximal value of 500 meV (band gap difference between Si and Ge) as x increases.

Because Si has an anisotropic dispersion relation, we emphasize electrons lying in the three different pairs of valley states generally experience different confinement potentials. To account for this effect, we fix the z direction to be aligned to the fin and the y direction to be perpendicular to the substrate, see Fig. 1. We also restrict ourselves to the analysis of Si [001], with fins that are aligned to the [110] crystallographic axis, i.e., $y\|[001]$ and $z\|[110]$. This is the standard orientation of current devices [1,2,4,84].

Shear-strain-induced lifting of the valley degeneracy.—The Hamiltonian in Eq. (1) allows us to accurately analyze the physics of conduction-band electrons in the fins shown in Fig. 1. We discretize H for different cross sections with lattice spacings a_x and a_y and we analyze the dispersion relation of the lowest energy states. Importantly, we include the inhomogeneous strain tensor $\underline{\boldsymbol{\varepsilon}}$ simulated by FEM with COMSOL Multiphysics® [85]; see SM [78].

The effect of strain in our fins is illustrated in Fig. 2(a), where we show the projection of the three-dimensional (3D) bulk valleys in Si onto the 1D BZ along $z\|[110]$. Along z, the four bulk Si valleys belonging to the xz plane (purple ellipses) are projected close to the X points and the two valleys along the $y\|[001]$ axis (turquoise circles) onto the Γ point ($k_z = 0$). When $\underline{\boldsymbol{\varepsilon}} = 0$ (dashed gray lines) all valleys are close in energy up to a small contribution caused by the anisotropic confinement. In analogy to planar heterostructures [63,65,77,86] at finite values $\underline{\boldsymbol{\varepsilon}}$ (blue solid lines) uniaxial strain splits away the states with minimum close to the X points by several tens of meV.

Shear strain results in the splitting of the remaining two valleys. A closeup into the dispersion relation in the vicinity of Γ, highlighting the shear-strain-induced

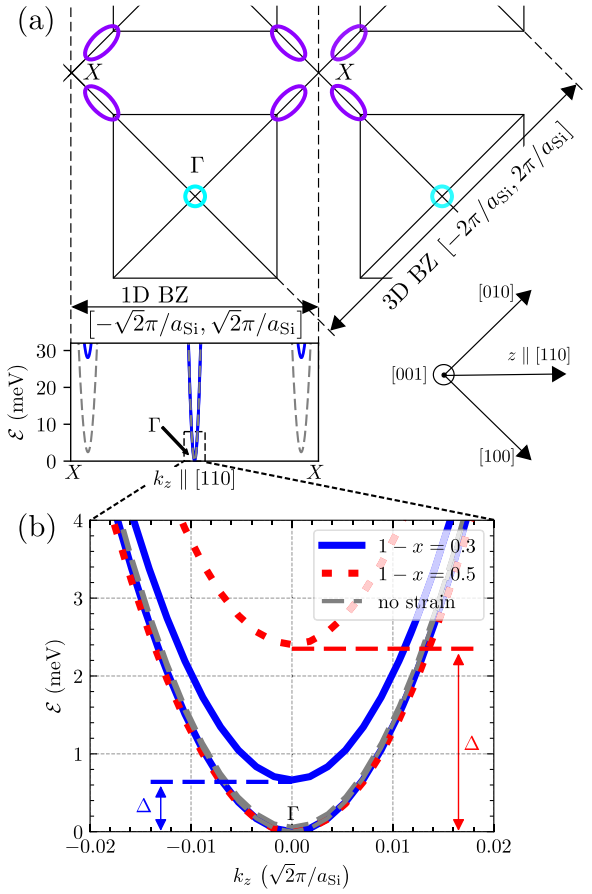

FIG. 2. Band dispersion of electrons confined in strained Si fins. (a) Projection of the six valleys of the 3D BZ of bulk Si onto the 1D BZ with momentum $k_z \| [110]$. The purple ellipses indicate the four valleys in the xz plane, while the turquoise circles indicate the two valleys near the X points in the out-of-plane direction y. At the bottom, we show the dispersion relation $\mathcal{E}(k_z)$ of the lowest pair of sub-bands at the 1D Γ point and close to the X point of the triangular Si fin sketched in Fig. 1(a). Without strain (dashed gray lines) all the states are close in energy. Including moderate strain induced by a Si_xGe_{1-x} alloy with $x = 0.7$ (solid blue lines), we observe that uniaxial strain ε_{ll} pushes the states with minimum at finite k_z several tens of meV away and shear strain $\varepsilon_{t_1t_2}$ induces a gap in the remaining two valleys in the y direction (turquoise circles). (b) Zoom into dispersion relation around the 1D Γ point. When $\varepsilon_{t_1t_2} = 0$, the two valleys are quasidegenerate. The degeneracy is lifted by shear strain induced by Si_xGe_{1-x}. The resulting energy gap $\Delta \sim 1$ meV increases with decreasing concentration of Si x, as shown by the blue and red lines obtained for $x = 0.7$ and $x = 0.5$, respectively. The dispersion relation is qualitatively similar for the strained fin in Fig. 1(b). We used $L_1 = 9.5$ nm, $L_2 = 19$ nm, $E_y = 1$ V μm^{-1} (pointing along [001]), $a_x = 0.32$ nm, and $a_y = 0.28$ nm.

valley splitting Δ, is shown in Fig. 2(b). We focus here on the triangular fin sketched in Fig. 1(a); however, the results discussed are valid also for rectangular fins. In the absence of strain the shear strain element $\varepsilon_{t_1t_2} = 0$ and the lowest two energy states (dashed gray line) are quasidegenerate [56,87], see Eq. (1). The Si_xGe_{1-x} induces a finite $\varepsilon_{t_1t_2}$ in the Si shell which lifts the valley degeneracy. Details on the strain profile in our fins are provided in Fig. 3 and the SM [78]. Considering a moderate Ge concentration of $1-x = 0.3$, we estimate $\Delta = 0.65$ meV for $E_y = 1$ V μm^{-1} pointing along [001], significantly larger than what is obtained in planar heterostructures [38–45]. By increasing the Ge amount to $1-x = 0.5$, $\varepsilon_{t_1t_2}$ increases [see Eq. (2)] and consequently a larger value of $\Delta = 2.35$ meV is reached. The split states from the same sub-band at $k_z = 0$ are strongly hybridized.

Because the electron is localized at the top of the fin, the substrate does not affect the values of Δ. We emphasize in striking contrast to valley splittings arising in planar heterostructures, our Δ arises from shear strain and therefore is reproducible and robust against atomistic disorder at the Si/SiGe interfaces [36,88] and modifications of the cross section (see SM [78]).

Electric-field dependence of valley splitting.—In planar Si/SiGe structures, the valley splitting Δ strongly depends on the applied electric field E. We show that in our fins, Δ can also be tuned *in situ* by E; however at large enough concentrations of Ge in the Si_xGe_{1-x} alloy, Δ remains large.

The dependence of Δ on E and $1-x$ is analyzed in Figs. 3(a) and 3(e). In the triangular fin sketched in Fig. 1(a), a positive electric field tends to decrease Δ. This trend can be understood by observing that E shifts the wave function toward the upper tip of the Si shell [see Figs. 3(b)–3(d)], where shear strain first decreases and then slightly increases with opposite sign, see Fig. 3(j). A detailed explanation of FEM simulations is provided in the SM [78]. As the concentration of Ge increases, strain also increases, resulting in $\Delta \gtrsim 15$ meV for a wide range of E. Because Δ depends on shear strain, our results are robust against variations in the shape of the cross section, which we verify in the SM [78].

Large values of Δ also emerge for a wide range of parameters in the rectangular Si fins on a SiGe substrate sketched in Fig. 1(b). Similar Si nanostructures are current state-of-the-art for spin qubits [4,84,89,90] and can be adapted to our proposal by replacing the oxide substrate by SiGe. In this device, we observe in Figs. 3(e)–3(i) a nontrivial interplay of $1-x$ and E, which we relate to the position and spacial spread of the wave function in the cross section. In this case, we study the effect of an electric field E pushing the electron wave function toward the upper-right corner of the fin; due to symmetry, the results are equivalent if the electric field pushes the electron toward the upper-left corner. In particular, $\varepsilon_{t_1t_2}$ is maximal at the left and right bottom sides of the fin, see Fig. 3(k), and, thus, Δ is large when the electron is localized close to these areas. We should emphasize, however, that when it is too close to the interface the electron risks leaking into the substrate. In addition, the QD is also easier to control electrostatically when it is localized at an upper corner.

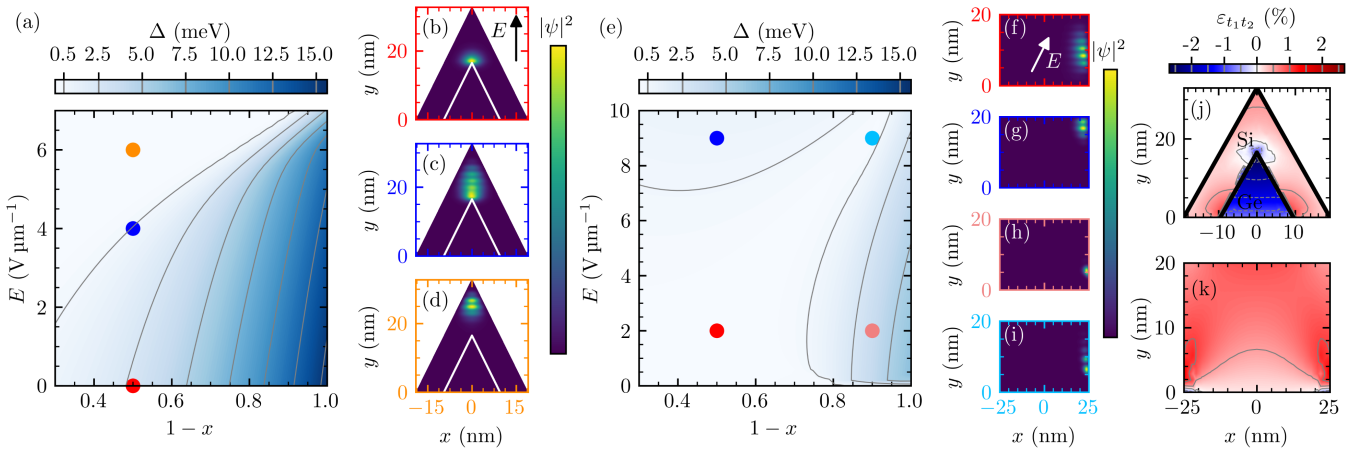

FIG. 3. Valley splitting Δ in Si/Si_xGe_{1-x} fins: (a) Δ against Ge concentration $1-x$ and electric field E in the triangular fin sketched in Fig. 1(a). For a wide range of experimentally relevant parameters $\Delta \gtrsim 0.5$ meV, substantially larger than in planar heterostructures; Δ is maximized when shear strain increases, i.e., at $1-x=1$, and at small values of E. The isocontours are defined in the colorbar. (b)–(d) Probability densities $|\psi|^2$ of electron wave function at $1-x=0.5$ for (b) $E=0$, (c) $E=4$ V μm^{-1}, and (d) $E=6$ V μm^{-1}, marked in (a). The inhogomeneous uniaxial strain localizes the electron at the top of the fin. At $E=0$ the electron lies at the Si/SiGe interface, where shear strain is maximal, and resulting in the largest Δ. Increasing the electric field the electron is pushed toward the tip of the Si shell, where shear strain is weaker and Δ decreases. We used $L_1=9.5$ nm and $L_2=19$ nm, as in Fig. 2. The same quantities (e) Δ, and (f)–(i) $|\psi|^2$ in the rectangular fin sketched in Fig. 1(b). Note the different directions of E in the two setups indicated by the arrows in (b) and (f). Here shear strain is larger at the left and right sides of the cross section. At $1-x<0.75$ and for small E the electron is localized at the bottom of the cross section (not shown). (f) At $1-x=0.5$ and $E=2$ V μm^{-1}, the electron is weakly localized at the right of the fin, resulting in $\Delta<0.5$ meV. (g) At $1-x=0.5$ and $E=9$ V μm^{-1}, the electron is pushed toward the upper-right corner of the fin and the valley splitting increases to $\Delta>0.5$ meV. (h) At $1-x=0.9$ and $E=2$ V μm^{-1}, the larger concentration of Ge enhances locally the strain at the bottom corner of the rectangle. (i) At $1-x=0.9$ and $E=9$ V μm^{-1}, the large values of E in a strongly strained device cause the wave function to spread out across the side. Then the situation is similar to (f) and $\Delta<0.5$ meV. We used $L_x=50$ nm, $L_y=20$ nm, $a_x=0.28$ nm, and $a_y=0.34$ nm. (j),(k) Shear strain $\varepsilon_{t_1t_2}$ simulated with FEM for the two devices for pure Ge instead of SiGe. (j) $\varepsilon_{t_1t_2}$ is large above the tip of the inner Ge fin and becomes first weaker toward the tip of the Si shell and then increases with opposite sign. (k) Large $\varepsilon_{t_1t_2}$ is found close to the left and right side of the Si slab. In case of $1-x=0.3$ the range of the color bar for (j),(k) is $[-0.82\%, 0.82\%]$. In the SM [78], we report cuts through (a) and (e) at certain values of $1-x$ and misaligned electric fields as well as a larger version of (j) and (k) and the strain simulation parameters used for our simulations.

For low concentrations of Ge ($1-x \lesssim 0.7$) electrons are localized at the upper corner of the cross section by a strong field E, and thus Δ increases with increasing E. For weak E the wave function is spread over the right side and Δ is small. At larger values of $1-x \gtrsim 0.7$, the inhomogeneous uniaxial strain localizes the electrons close to the edges already at weak E, thus resulting in large values of Δ. In this case, Δ is only weakly dependent on E, and it decreases with increasing E because the electrons are pushed away from the substrate. Details on the electric field dependence are provided in the SM [78].

The large valley splitting due to shear strain has important consequences for spin qubits realized in gate-defined QDs in Si fins. The spin qubit lifetime in planar Si/SiGe heterostructures is strongly limited at spin-valley relaxation hot spots where the qubit Zeeman and valley splittings become comparable [41,49,50,56,91]. These hot spots are naturally avoided in our devices because of the large difference between the typically small qubit Zeeman splitting of ∼10 μeV and the valley splitting of ∼1–10 meV we predict.

Finally, we note that in quantum dot devices, an additional shear strain contribution arises because of the oxide and gate stacking. The shear strain values are strongly device dependent but simulations in Si/Ge heterostructures estimate these terms to be approximately one order of magnitude smaller than the values predicted here [92,93]. As a result, we expect that gate-induced strain will only weakly renormalize the large valley splitting in our devices.

Conclusion.—In this work we show that shear strain substantially enhances the valley splitting in Si/SiGe heterostructures. In realistic Si fins we predict valley splittings ∼1–10 meV, orders of magnitude larger than in current devices. We show that the amplitude of the gap can be engineered by varying the composition of the Si_xGe_{1-x} alloy and is controllable *in situ* by electric fields. Importantly, due to the large valley splitting, spin-valley relaxation hot spots are avoided naturally in our proposed Si fins. Our designs are robust against variations of the fin shape and, in contrast to planar systems, not affected by atomistic disorder. By removing a critical issue of current electron spin qubits in Si, our devices will push these

architectures toward new coherence standards and pave the way toward large-scale semiconductor-based quantum processors.

We thank Dominik Zumbühl for giving access to the license for COMSOL Multiphysics® and Andreas V. Kuhlmann for useful comments. This work was supported as a part of NCCR SPIN, a National Centre of Competence (or Excellence) in Research, funded by the Swiss National Science Foundation (Grant No. 51NF40-180604).

*Contact author: ch.adelsberger@gmail.com
†Present address: QuTech and Kavli Institute of Nanoscience, Delft University of Technology, Lorentzweg 1, 2628 CJ Delft, Netherlands.

[1] S. Geyer, B. Hetényi, S. Bosco, L. C. Camenzind, R. S. Eggli, A. Fuhrer, D. Loss, R. J. Warburton, D. M. Zumbühl, and A. V. Kuhlmann, Nat. Phys. (2024).
[2] L. C. Camenzind, S. Geyer, A. Fuhrer, R. J. Warburton, D. M. Zumbühl, and A. V. Kuhlmann, Nat. Electron. Rev. **5**, 178 (2022).
[3] N. W. Hendrickx, W. I. L. Lawrie, M. Russ, F. van Riggelen, S. L. de Snoo, R. N. Schouten, A. Sammak, G. Scappucci, and M. Veldhorst, Nature (London) **591**, 580 (2021).
[4] N. Piot, B. Brun, V. Schmitt, S. Zihlmann, V. P. Michal, A. Apra, J. C. Abadillo-Uriel, X. Jehl, B. Bertrand, H. Niebojewski, L. Hutin, M. Vinet, M. Urdampilleta, T. Meunier, Y.-M. Niquet, R. Maurand, and S. D. Franceschi, Nat. Nanotechnol. **17**, 1072 (2022).
[5] D. Jirovec, A. Hofmann, A. Ballabio, P. M. Mutter, G. Tavani, M. Botifoll, A. Crippa, J. Kukucka, O. Sagi, F. Martins, J. Saez-Mollejo, I. Prieto, M. Borovkov, J. Arbiol, D. Chrastina, G. Isella, and G. Katsaros, Nat. Mater. **20**, 1106 (2021).
[6] D. Jirovec, P. M. Mutter, A. Hofmann, A. Crippa, M. Rychetsky, D. L. Craig, J. Kukucka, F. Martins, A. Ballabio, N. Ares, D. Chrastina, G. Isella, G. Burkard, and G. Katsaros, Phys. Rev. Lett. **128**, 126803 (2022).
[7] M. T. Mądzik *et al.*, Nature (London) **601**, 348 (2022).
[8] L. Petit, M. Russ, G. H. G. J. Eenink, W. I. L. Lawrie, J. S. Clarke, L. M. K. Vandersypen, and M. Veldhorst, Commun. Mater. **3**, 82 (2022).
[9] S. G. J. Philips, M. T. Mądzik, S. V. Amitonov, S. L. de Snoo, M. Russ, N. Kalhor, C. Volk, W. I. L. Lawrie, D. Brousse, L. Tryputen, B. P. Wuetz, A. Sammak, M. Veldhorst, G. Scappucci, and L. M. K. Vandersypen, Nature (London) **609**, 919 (2022).
[10] F. K. Unseld, M. Meyer, M. T. Mądzik, F. Borsoi, S. L. de Snoo, S. V. Amitonov, A. Sammak, G. Scappucci, M. Veldhorst, and L. M. K. Vandersypen, Appl. Phys. Lett. **123**, 084002 (2023).
[11] A. O. Denisov, S. W. Oh, G. Fuchs, A. R. Mills, P. Chen, C. R. Anderson, M. F. Gyure, A. W. Barnard, and J. R. Petta, Nano Lett. **22**, 4807 (2022).
[12] K. Takeda, A. Noiri, J. Yoneda, T. Nakajima, and S. Tarucha, Phys. Rev. Lett. **124**, 117701 (2020).
[13] X. Xue, M. Russ, N. Samkharadze, B. Undseth, A. Sammak, G. Scappucci, and L. M. K. Vandersypen, Nature (London) **601**, 343 (2022).
[14] K. M. Itoh and H. Watanabe, MRS Commun. **4**, 143 (2014).
[15] M. Veldhorst, J. C. C. Hwang, C. H. Yang, A. W. Leenstra, B. de Ronde, J. P. Dehollain, J. T. Muhonen, F. E. Hudson, K. M. Itoh, A. Morello, and A. S. Dzurak, Nat. Nanotechnol. **9**, 981 (2014).
[16] K. Takeda, J. Kamioka, T. Otsuka, J. Yoneda, T. Nakajima, M. R. Delbecq, S. Amaha, G. Allison, T. Kodera, S. Oda, and S. Tarucha, Sci. Adv. **2**, e1600694 (2016).
[17] J. Yoneda, K. Takeda, T. Otsuka, T. Nakajima, M. R. Delbecq, G. Allison, T. Honda, T. Kodera, S. Oda, Y. Hoshi, N. Usami, K. M. Itoh, and S. Tarucha, Nat. Nanotechnol. **13**, 102 (2018).
[18] M. Veldhorst, C. H. Yang, J. C. C. Hwang, W. Huang, J. P. Dehollain, J. T. Muhonen, S. Simmons, A. Laucht, F. E. Hudson, K. M. Itoh, A. Morello, and A. S. Dzurak, Nature (London) **526**, 410 (2015).
[19] D. M. Zajac, T. M. Hazard, X. Mi, E. Nielsen, and J. R. Petta, Phys. Rev. Appl. **6**, 054013 (2016).
[20] T. F. Watson, S. G. J. Philips, E. Kawakami, D. R. Ward, P. Scarlino, M. Veldhorst, D. E. Savage, M. G. Lagally, M. Friesen, S. N. Coppersmith, M. A. Eriksson, and L. M. K. Vandersypen, Nature (London) **555**, 633 (2018).
[21] W. Huang, C. H. Yang, K. W. Chan, T. Tanttu, B. Hensen, R. C. C. Leon, M. A. Fogarty, J. C. C. Hwang, F. E. Hudson, K. M. Itoh, A. Morello, A. Laucht, and A. S. Dzurak, Nature (London) **569**, 532 (2019).
[22] X. Xue, T. F. Watson, J. Helsen, D. R. Ward, D. E. Savage, M. G. Lagally, S. N. Coppersmith, M. A. Eriksson, S. Wehner, and L. M. K. Vandersypen, Phys. Rev. X **9**, 021011 (2019).
[23] A. J. Sigillito, J. C. Loy, D. M. Zajac, M. J. Gullans, L. F. Edge, and J. R. Petta, Phys. Rev. Appl. **11**, 061006(R) (2019).
[24] X. Mi, M. Benito, S. Putz, D. M. Zajac, J. M. Taylor, G. Burkard, and J. R. Petta, Nature (London) **555**, 599 (2018).
[25] N. Samkharadze, G. Zheng, N. Kalhor, D. Brousse, A. Sammak, U. C. Mendes, A. Blais, G. Scappucci, and L. M. K. Vandersypen, Science **359**, 1123 (2018).
[26] T. Bonsen, P. Harvey-Collard, M. Russ, J. Dijkema, A. Sammak, G. Scappucci, and L. M. K. Vandersypen, Phys. Rev. Lett. **130**, 137001 (2023).
[27] R. Li, L. Petit, D. P. Franke, J. P. Dehollain, J. Helsen, M. Steudtner, N. K. Thomas, Z. R. Yoscovits, K. J. Singh, S. Wehner, L. M. K. Vandersypen, J. S. Clarke, and M. Veldhorst, Sci. Adv. **4**, eaar3960 (2018).
[28] A. R. Mills, D. M. Zajac, M. J. Gullans, F. J. Schupp, T. M. Hazard, and J. R. Petta, Nat. Commun. **10**, 1063 (2019).
[29] A. Noiri, K. Takeda, T. Nakajima, T. Kobayashi, A. Sammak, G. Scappucci, and S. Tarucha, Nat. Commun. **13**, 5740 (2022).
[30] I. Seidler, T. Struck, R. Xue, N. Focke, S. Trellenkamp, H. Bluhm, and L. R. Schreiber, npj Quantum Inf. **8**, 100 (2022).
[31] K. Takeda, A. Noiri, T. Nakajima, J. Yoneda, T. Kobayashi, and S. Tarucha, Nat. Nanotechnol. **16**, 965 (2021).
[32] A. R. Mills, C. R. Guinn, M. M. Feldman, A. J. Sigillito, M. J. Gullans, M. T. Rakher, J. Kerckhoff, C. A. C. Jackson, and J. R. Petta, Phys. Rev. Appl. **18**, 064028 (2022).

[33] A. Noiri, K. Takeda, T. Nakajima, T. Kobayashi, A. Sammak, G. Scappucci, and S. Tarucha, Nature (London) **601**, 338 (2022).
[34] T. Tanttu *et al.*, arXiv:2303.04090v2.
[35] T. Ando, A. B. Fowler, and F. Stern, Rev. Mod. Phys. **54**, 437 (1982).
[36] F. A. Zwanenburg, A. S. Dzurak, A. Morello, M. Y. Simmons, L. C. L. Hollenberg, G. Klimeck, S. Rogge, S. N. Coppersmith, and M. A. Eriksson, Rev. Mod. Phys. **85**, 961 (2013).
[37] R. Ruskov, M. Veldhorst, A. S. Dzurak, and C. Tahan, Phys. Rev. B **98**, 245424 (2018).
[38] M. G. Borselli, R. S. Ross, A. A. Kiselev, E. T. Croke, K. S. Holabird, P. W. Deelman, L. D. Warren, I. Alvarado-Rodriguez, I. Milosavljevic, F. C. Ku, W. S. Wong, A. E. Schmitz, M. Sokolich, M. F. Gyure, and A. T. Hunter, Appl. Phys. Lett. **98**, 123118 (2011).
[39] Z. Shi, C. B. Simmons, J. R. Prance, J. K. Gamble, M. Friesen, D. E. Savage, M. G. Lagally, S. N. Coppersmith, and M. A. Eriksson, Appl. Phys. Lett. **99**, 233108 (2011).
[40] D. M. Zajac, T. M. Hazard, X. Mi, K. Wang, and J. R. Petta, Appl. Phys. Lett. **106**, 223507 (2015).
[41] A. Hollmann, T. Struck, V. Langrock, A. Schmidbauer, F. Schauer, T. Leonhardt, K. Sawano, H. Riemann, N. V. Abrosimov, D. Bougeard, and L. R. Schreiber, Phys. Rev. Appl. **13**, 034068 (2020).
[42] E. H. Chen, K. Raach, A. Pan, A. A. Kiselev, E. Acuna, J. Z. Blumoff, T. Brecht, M. D. Choi, W. Ha, D. R. Hulbert, M. P. Jura, T. E. Keating, R. Noah, B. Sun, B. J. Thomas, M. G. Borselli, C. A. C. Jackson, M. T. Rakher, and R. S. Ross, Phys. Rev. Appl. **15**, 044033 (2021).
[43] P. Scarlino, E. Kawakami, T. Jullien, D. R. Ward, D. E. Savage, M. G. Lagally, M. Friesen, S. N. Coppersmith, M. A. Eriksson, and L. M. K. Vandersypen, Phys. Rev. B **95**, 165429 (2017).
[44] X. Mi, S. Kohler, and J. R. Petta, Phys. Rev. B **98**, 161404 (R) (2018).
[45] X. Mi, C. G. Péterfalvi, G. Burkard, and J. R. Petta, Phys. Rev. Lett. **119**, 176803 (2017).
[46] M. Friesen, S. Chutia, C. Tahan, and S. N. Coppersmith, Phys. Rev. B **75**, 115318 (2007).
[47] S. Chutia, S. N. Coppersmith, and M. Friesen, Phys. Rev. B **77**, 193311 (2008).
[48] A. L. Saraiva, M. J. Calderón, X. Hu, S. Das Sarma, and B. Koiller, Phys. Rev. B **80**, 081305(R) (2009).
[49] A. Hosseinkhani and G. Burkard, Phys. Rev. Res. **2**, 043180 (2020).
[50] A. Hosseinkhani and G. Burkard, Phys. Rev. B **104**, 085309 (2021).
[51] J. R. F. Lima and G. Burkard, Mater. Quantum. Technol. **3**, 025004 (2023).
[52] B. P. Wuetz, M. P. Losert, S. Koelling, L. E. A. Stehouwer, A.-M. J. Zwerver, S. G. J. Philips, M. T. Mądzik, X. Xue, G. Zheng, M. Lodari, S. V. Amitonov, N. Samkharadze, A. Sammak, L. M. K. Vandersypen, R. Rahman, S. N. Coppersmith, O. Moutanabbir, M. Friesen, and G. Scappucci, Nat. Commun. **13**, 7730 (2022).
[53] C. H. Yang, R. C. C. Leon, J. C. C. Hwang, A. Saraiva, T. Tanttu, W. Huang, J. C. Lemyre, K. W. Chan, K. Y. Tan, F. E. Hudson, K. M. Itoh, A. Morello, M. Pioro-Ladrière, A. Laucht, and A. S. Dzurak, Nature (London) **580**, 350 (2020).
[54] T. McJunkin, B. Harpt, Y. Feng, M. P. Losert, R. Rahman, J. P. Dodson, M. A. Wolfe, D. E. Savage, M. G. Lagally, S. N. Coppersmith, M. Friesen, R. Joynt, and M. A. Eriksson, Nat. Commun. **13**, 7777 (2022).
[55] B. D. Woods, M. A. Eriksson, R. Joynt, and M. Friesen, Phys. Rev. B **107**, 035418 (2023).
[56] C. H. Yang, A. Rossi, R. Ruskov, N. S. Lai, F. A. Mohiyaddin, S. Lee, C. Tahan, G. Klimeck, A. Morello, and A. S. Dzurak, Nat. Commun. **4**, 2069 (2013).
[57] A. Saraiva, W. H. Lim, C. H. Yang, C. C. Escott, A. Laucht, and A. S. Dzurak, Adv. Funct. Mater. **32**, 2105488 (2021).
[58] J. D. Cifuentes *et al.*, arXiv:2303.14864.
[59] S. Choudhary, M. Yogesh, D. Schwarz, H. S. Funk, S. Ghosh, S. K. Sharma, J. Schulze, and K. E. Gonsalves, J. Vac. Sci. Technol. B **41**, 052203 (2023).
[60] S. P. Ramanandan, J. Reñé Sapera, A. Morelle, S. Martí-Sánchez, A. Rudra, J. Arbiol, V. G. Dubrovskii, and A. Fontcuberta i Morral, Nanoscale Horiz. **9**, 555 (2024).
[61] R. R. Reeber and K. Wang, Mater. Chem. Phys. **46**, 259 (1996).
[62] J. C. Hensel, H. Hasegawa, and M. Nakayama, Phys. Rev. **138**, A225 (1965).
[63] Z. Stanojevic, O. Baumgartner, V. Sverdlov, and H. Kosina, in *2010 14th International Workshop on Computational Electronics* (IEEE, 2010).
[64] V. Sverdlov, G. Karlowatz, S. Dhar, H. Kosina, and S. Selberherr, Solid-State Electron. **52**, 1563 (2008).
[65] M. V. Fischetti and S. E. Laux, J. Appl. Phys. **80**, 2234 (1996).
[66] C. G. Van de Walle and R. M. Martin, Phys. Rev. B **34**, 5621 (1986).
[67] C. Tserbak, H. M. Polatoglou, and G. Theodorou, Phys. Rev. B **47**, 7104 (1993).
[68] P. Friedel, M. S. Hybertsen, and M. Schlüter, Phys. Rev. B **39**, 7974 (1989).
[69] I. Balslev, Phys. Rev. **143**, 636 (1966).
[70] M. M. Rieger and P. Vogl, Phys. Rev. B **48**, 14276 (1993).
[71] I. Goroff and L. Kleinman, Phys. Rev. **132**, 1080 (1963).
[72] L. D. Laude, F. H. Pollak, and M. Cardona, Phys. Rev. B **3**, 2623 (1971).
[73] Z. Li, P. Graziosi, and N. Neophytou, Phys. Rev. B **104**, 195201 (2021).
[74] S. Bosco and D. Loss, Phys. Rev. Appl. **18**, 044038 (2022).
[75] C. Kloeffel, M. Trif, and D. Loss, Phys. Rev. B **90**, 115419 (2014).
[76] A. M. Kosevich, E. M. Lifshitz, L. D. Landau, and L. P. Pitaevskii, *Theory of Elasticity* (Butterworth-Heinemann, Oxford, 1986), Vol. 7.
[77] Y.-M. Niquet, C. Delerue, and C. Krzeminski, Nano Lett. **12**, 3545 (2012).
[78] See Supplemental Material at http://link.aps.org/supplemental/10.1103/PhysRevLett.133.037001, which includes Refs. [79–81], for a discussion of the model for strain used for FEM calculations and results for the uniaxial strain components, atomic size steps at the interface between the Ge fin and the Si shell, more details on the electric field dependence of the valley splitting, a discussion of the robustness of the valley splitting, and a semicylindrical

device where a sizable valley splitting is found in a broad parameter regime of electric field strengths and Ge concentrations as well.

[79] H. T. Mengistu and A. García-Cristóbal, Int. J. Solids Struct. **100–101**, 257 (2016).

[80] H. J. McSkimin and P. Andreatch, J. Appl. Phys. **35**, 2161 (1964).

[81] H. J. McSkimin and P. Andreatch, J. Appl. Phys. **34**, 651 (1963).

[82] S. Bosco, M. Benito, C. Adelsberger, and D. Loss, Phys. Rev. B **104**, 115425 (2021).

[83] L. A. Terrazos, E. Marcellina, Z. Wang, S. N. Coppersmith, M. Friesen, A. R. Hamilton, X. Hu, B. Koiller, A. L. Saraiva, D. Culcer, and R. B. Capaz, Phys. Rev. B **103**, 125201 (2021).

[84] R. Maurand, X. Jehl, D. Kotekar-Patil, A. Corna, H. Bohuslavskyi, R. Laviéville, L. Hutin, S. Barraud, M. Vinet, M. Sanquer, and S. D. Franceschi, Nat. Commun. **7**, 13575 (2016).

[85] COMSOL Multiphysics® v. 6.1. www.comsol.com. COMSOL AB, Stockholm, Sweden.

[86] K.-H. Hong, J. Kim, S.-H. Lee, and J. K. Shin, Nano Lett. **8**, 1335 (2008).

[87] P. Huang and X. Hu, Phys. Rev. B **90**, 235315 (2014).

[88] T. B. Boykin, G. Klimeck, M. A. Eriksson, M. Friesen, S. N. Coppersmith, P. von Allmen, F. Oyafuso, and S. Lee, Appl. Phys. Lett. **84**, 115 (2004).

[89] C. X. Yu, S. Zihlmann, J. C. Abadillo-Uriel, V. P. Michal, N. Rambal, H. Niebojewski, T. Bedecarrats, M. Vinet, É. Dumur, M. Filippone, B. Bertrand, S. D. Franceschi, Y.-M. Niquet, and R. Maurand, Nat. Nanotechnol. **18**, 741 (2023).

[90] M. F. Gonzalez-Zalba, S. de Franceschi, E. Charbon, T. Meunier, M. Vinet, and A. S. Dzurak, Nat. Electron. **4**, 872 (2021).

[91] F. Borjans, D. M. Zajac, T. M. Hazard, and J. R. Petta, Phys. Rev. Appl. **11**, 044063 (2019).

[92] S. Asaad, V. Mourik, B. Joecker, M. A. I. Johnson, A. D. Baczewski, H. R. Firgau, M. T. Mądzik, V. Schmitt, J. J. Pla, F. E. Hudson, K. M. Itoh, J. C. McCallum, A. S. Dzurak, A. Laucht, and A. Morello, Nature (London) **579**, 205 (2020).

[93] J. C. Abadillo-Uriel, E. A. Rodriguez-Mena, B. Martinez, and Y.-M. Niquet, Phys. Rev. Lett. **131**, 097002 (2023).